

Malaria Parasitic Detection using a New Deep Boosted and Ensemble Learning Framework

Saddam Hussain Khan^{1*}

¹Department of Computer Systems Engineering, University of Engineering and Applied Sciences (UEAS), Swat 19060, Pakistan,
Corresponding author: (e-mail: saddamhkh@ueas.edu.pk).

Abstract

Malaria is a potentially fatal plasmodium parasite injected by female anopheles mosquitoes that infect red blood cells and millions worldwide yearly. However, specialists' manual screening in clinical practice is laborious and prone to error. Therefore, a novel Deep Boosted and Ensemble Learning (DBEL) framework, comprising the stacking of new Boosted-BR-STM convolutional neural networks (CNN) and ensemble classifiers, is developed to screen malaria parasite images. The proposed STM-SB-BRNet is based on a new dilated-convolutional block-based split transform merge (STM) and feature-map Squeezing-Boosting (SB) ideas. Moreover, the new STM block uses regional and boundary operations to learn the malaria parasite's homogeneity, heterogeneity, and boundary with patterns. Furthermore, the diverse boosted channels are attained by employing Transfer Learning-based new feature-map SB in STM blocks at the abstract, medium, and conclusion levels to learn minute intensity and texture variation of the parasitic pattern. The proposed DBEL framework implicates the stacking of prominent and diverse boosted channels and provides the generated discriminative features of the developed Boosted-BR-STM to the ensemble of ML classifiers. The proposed framework improves the discrimination ability and generalization of ensemble learning. Moreover, the deep feature spaces of the developed Boosted-BR-STM and customized CNNs are fed into ML classifiers for comparative analysis. The proposed DBEL framework outperforms the existing techniques on the NIH malaria dataset that are enhanced using discrete wavelet transform to enrich feature space. The proposed DBEL framework achieved accuracy (98.50%), sensitivity (0.9920), F-score (0.9850), and AUC (0.997), which suggest it to be utilized for malaria parasite screening.

Keywords: Screening, Squeezing, Boosting, Split-Transform and Merge, Transfer Learning, Malaria, Parasite.

1. Introduction

Malaria is a potentially fatal disease caused by a female Anopheles mosquito that injects plasmodium parasites with one nasty bite. In most cases, plasmodium parasites target healthy red blood cells (RBC) around one or two weeks after their emergence in the human body [1]. This bacterial infection is hazardous to kids, persons with impaired immune systems, pregnant women, and the elderly at risk [2]. P. Falciparum malaria is particularly dangerous to pregnant women as it increases stillbirth, maternal death, miscarriage, and newborn [3]. The World Health Organization reported roughly 241-million malaria suspects and 627000 fatalities in 2021. The African continent is perhaps the most afflicted, accounting for 95 % of 90% of deaths and 80% of child fatalities caused by malaria [4,5].

RBCs were microscopically examined in a thick, thin blood smear frequently used to identify malaria [6]. The thick and thin-smear test aids in identifying the density of parasites in a person's body and malaria species, respectively [7,8]. Expert pathologists manually analyze blood smear films to get a microscopic diagnosis. However, manual analysis is time-consuming, laborious, and unreliable [9]. Malaria candidates are usually seen in emerging countries, where classical lab facilities and other diagnostic tools are unavailable. In addition, a global shortage of trained professionals significantly impacts the healthcare systems of developing countries [10]. Therefore, a computer-based screening tool is essential for speedy and reliable malaria analysis [11].

Artificial intelligence (AI) and machine learning (ML) have aided in the development of malaria diagnostic methods that are effective and precise in processing large amounts of parasite-contaminated RBC samples [12]. Computer-based software will support clinicians in diagnosis and therapy, facilitating established lab practices [13,14]. However, this convention performed poorly on massive data and was incapable of learning complex patterns. Therefore, Deep Learning (DL) algorithms emerged and inspired researchers' interest in dealing with enormous amounts of data and learning complicated patterns. They have significant growth for medical imaging infection diagnosis [15–17].

Malaria parasite analysis is crucial for diagnosing infected cells. In this regard, a deep CNN-based identification helps quickly and accurately analyze malaria parasite images. Several CNN-based classification frameworks and experimental models have extensively been employed on the NIH malaria dataset to improve detection [18,19]. CNN extracts deep features automatically by avoiding the time-consuming hand-crafted feature extraction and reduces computational power [19,20].

In this study, we have proposed new deep hybrid learning comprised of novel Deep CNNs and ensemble learning to analyze malaria parasite-afflicted patients accurately and efficiently. The proposed deep Boosted-BR-STM exploits the channel Squeezing and Boosting (SB) technique with a novel Split Transform Merge (STM) block. Moreover, the developed STM block of deep Boosted-BR-STM uses the concept of homogenous and heterogeneous. The proposed framework and existing techniques are validated on a conventional NIH-malaria dataset. The significant contributions are as follows:

1. A new Deep Boosted and Ensemble Learning (DBEL) framework is proposed comprising a new Boosted-BR-STM CNN and ensemble learning for detecting RBCs infected with the plasmodium falciparum using blood smear images. The dataset is initially enhanced and reduced in dimension using a discrete wavelet transform (DWT) to improve computational complexity.
2. The proposed deep Boosted-BR-STM exploits the channel SB technique with a novel Split Transform Merge (STM) block. Moreover, the developed STM block of Boosted-BR-STM uses the concept of homogenous and heterogeneous.
3. The new idea SB is carefully employed in the new STM block at abstract, medium, and conclusion levels to capture the diverse pattern of homogeneous, heterogeneous, contrast, and textural variations of the parasitic cell. SB notion is utilized by merging reduced prominent channels with TL-based extracted additional feature maps to improve Boosted-BR-STM performances.
4. The proposed framework grants the inherent properties of diverse prominent and boosted channels to the discriminative feature level and fed to the ensemble of ML classifiers, improving the capability of

discrimination and generalization of ensemble learning. The ML classifiers' ensemble effectively reduces feature dimension and improves diverse decision space.

5. The proposed hybrid DBEL framework performance is compared to existing techniques utilized in NIH-malaria original and enhanced datasets.

The rest of the manuscript is arranged in the following ways. In sections 2 and 3, the remainder of the article discusses related work and the proposed malaria detection framework. Materials and implementation details are provided in Section 4. The performance analysis and outcomes are presented in Section 5. Finally, the article's conclusion is in Section 6.

2. Related Work

Several ML techniques were automatically determined in stained RBC samples employing methods over time [21]. ML algorithms such as Extreme-Learning Machine methods, Global White Balance, Logistic Regression, SVM, Adaptive Non-linear Grayscale, and KNN have enhanced classification performance [22,23]. The malaria parasite-infected features like RBCs, color, size, form, and statistical data were extracted and provided to ML algorithms [24,25]. Moreover, the deep belief network technique was used to classify the parasites, which yielded a 90.21 % accuracy [26]. The approaches mentioned above, on the other hand, indicated prediction accuracy in the range of 84–94 %.

Several researchers used deep CNN-based detection that automatically and quickly identifies cells infected with the malaria parasite, achieving a 91.5 % detection rate [31-33]. Medical datasets with labels are generally limited in size and thus unsuitable for practical application. Therefore, TL has been utilized in a limited labeled malaria dataset to forecast malaria parasites in RBC [27]. TL-based existing CNNs have been employed to improve and have attained accuracies of 75% to 94% [28–30]. Furthermore, an investigation on R-CNN for parasite identification has been carried out, with excellent results [31].

Previous studies employed VGG16 to identify malaria using the common NIH dataset and achieved 95.96 % accuracy [32]. The balanced NIH dataset included 27,556 images and was resized to 224 by 224 pixels. A sequential-tailored CNN was obtained with a 95.9 % F1 score, 94.7 % sensitivity, and 92.7% accuracy [20]. The existing ResNet50 yielded a 95.4 % accuracy using the malaria dataset [33]. Moreover, the custom-made CNN model demonstrated 96.82 % accuracy, 96.33 % using five convolutional and pooling layers, and 96.82 % F1-score [19]. Eventually, a hybrid platform that systematically reduces structural and empirical risk has been recently adopted and achieved a sensitivity of 93.44 % and an accuracy of 93.13 % [20,27]. However, there are certain limitations to the prior work:

Previous CNN models have been used to detect parasite images designed specifically for natural samples. In contrast, the medical images have distinct patterns and textures of the parasite malaria infection, limiting the model's performance. The prior research primarily focused on the accuracy of the validation dataset. Mostly, the previous studies are evaluated using accuracy; however, the results of a single-measure evaluation of the detecting system could be more reliable. Therefore, the detection rate and F-score are essential indicators of parasite detection. Moreover, testing evaluation measures on a vast, previously unseen test dataset is necessary for determining the detection model's robustness. Furthermore, several models have been evaluated on a limited dataset of images of malaria parasites.

3. Malaria Parasite Detection Scheme

The microscope analyzes malaria parasites from blood-films stained with various chemical stains [34]. Various scanners, chemical stains, concentrations, and methods can cause color differences. Therefore, analyzing parasite and artifact patterns become challenging and occur substantial margins error. These challenges necessitate designing a new deep CNN and ensemble learning framework to capture complicated patterns and identify malaria infectious microscopic thin smear samples. The developed framework comprised a new Boosted-BR-STM, ensemble learning, and contemporary customized

CNNs to screen parasite-infected cells from healthy images. The proposed malaria detection scheme utilizes three experimental arrangements: (1) the proposed DBEL and (2) the DBML framework, and (3) the evaluation of existing CNNs. These existing CNNs learned from scratch and fine-tuned using TL on the malaria NIH dataset. Moreover, these CNNs are evaluated as (i) The deep features are extracted from existing CNNs and provided to the ML classifier (ii) The Softmax-based evaluations. Additionally, the DWT and data augmentation as pre-processing techniques and detection CNNs are used to detect stain impurities or artifacts from parasite images and analyze different parasitic patterns. The overall workflow is arranged in Figure 1.

3.1. Data Enhancement

Discrete wavelet transformations (DWT) effectively produce salient feature maps and reduce noise [35]. DWT divides the image into four sub-parts: high, low, and diagonal-resolution channels. The next level of DWT, the low and diagonal-resolution channels, is stored and altered to provide the necessary DWT coefficients for parasite detection. Moreover, a 75 % dimension reduction at each level minimizes computational complexities. The low- and high-resolution images are combined and reconstructed using IDWT to produce highly informative (low-resolution and diagonal features) enhanced images [36]. The original and improved DWT data is shown in Figure 2.

3.2. Data Augmentation

Data augmentation is widely applied to boost the robustness of the model and lessens the risk of overfitting. Data instances are increased in runtime during the model training using different data augmentation techniques [37]. This work uses rotation, scaling, shearing, translation, and other standard data augmentation techniques, as shown in Table 1.

Table 1 Data Augmentation detail

Parameter	Values
Rotation	[\pm 5] degree
Shearing	[\pm 0.05]
X-Y Reflection	[\pm 1]

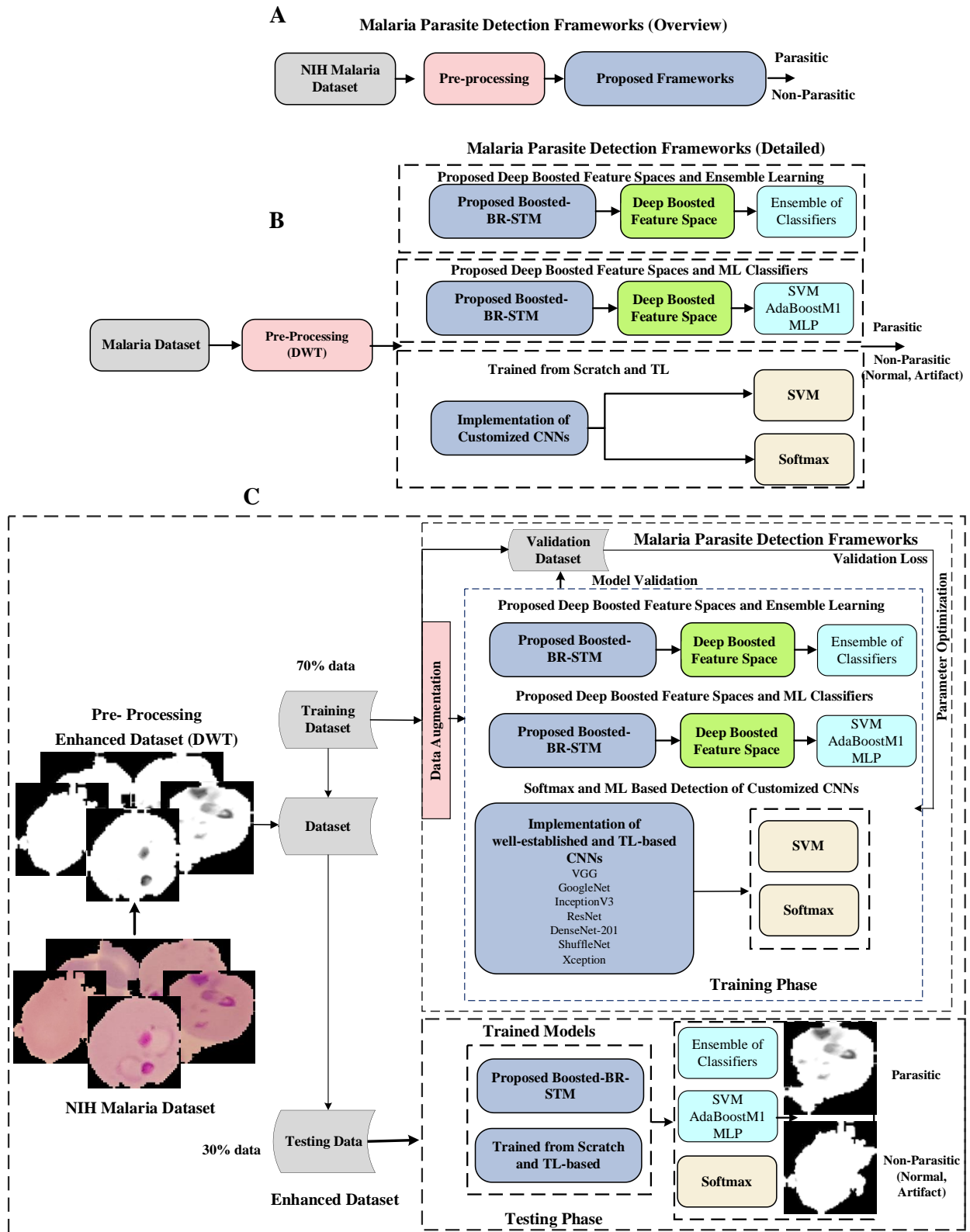


Figure 1 The flow diagram of the developed malaria parasite detection scheme

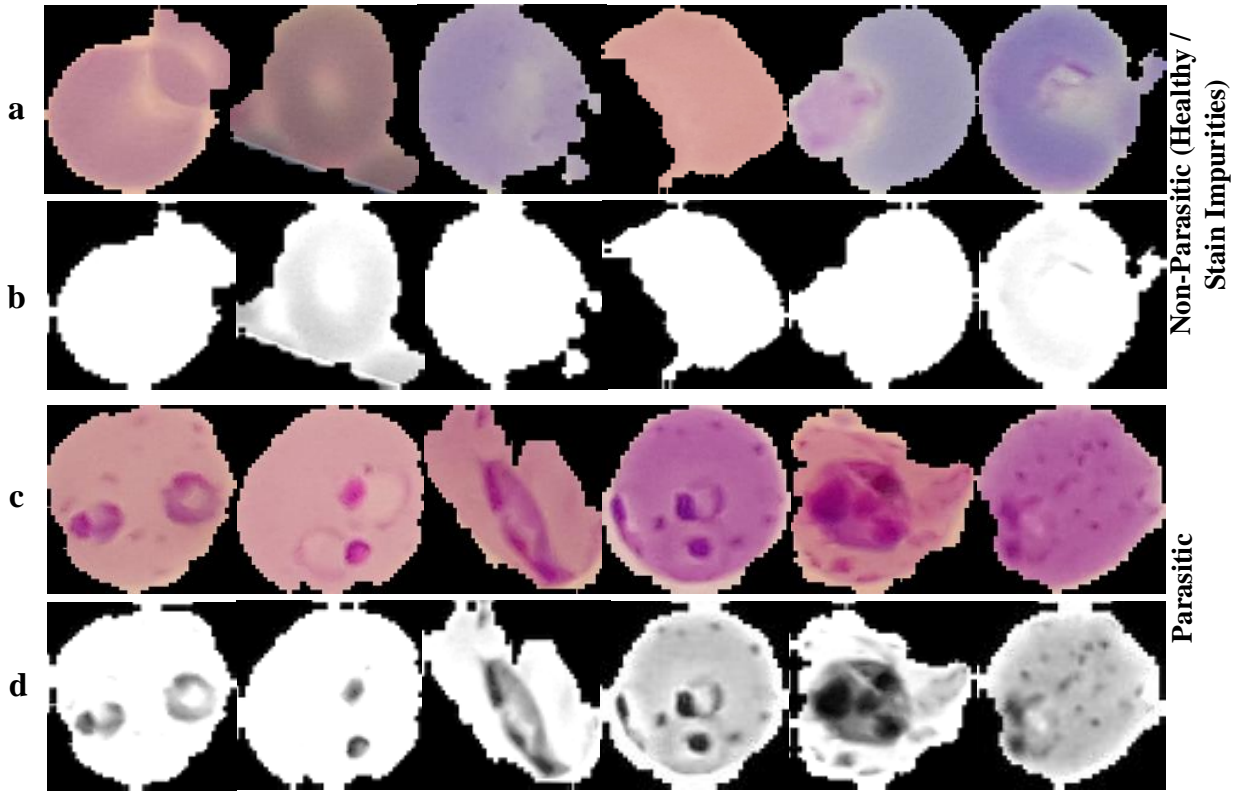


Figure 2 Parasite and Non-Parasite (healthy, stain artifact) samples from the NIH malaria dataset are shown in panels (a, c). While (b, d) displays their DWT-enhanced examples, respectively.

3.3. The Proposed Deep Boosted and Ensemble Learning Framework

This research proposes a new deep DBEL scheme that is comprised of the developed Boosted-BR-STM BRNet and ensemble techniques for malaria parasite detection. Moreover, the developed Boosted-BR-STM penultimate layers are used for deep feature extraction. The workflow of malaria parasite detection schemes is illustrated in Figure 3.

3.3.1. The Proposed Channel Boosted-BR-STM CNN

This work develops new Boosted-BR-STM CNNs to identify parasitic malaria patients. In the developed CNN, a novel STM-based convolution block is implemented in homogenous and boundary operations to look into regional homogenous and heterogeneous parasitic patterns. Moreover, the new SB ideas are employed in each STM block to attain the prominently reduced and diverse enhanced feature-maps. The channel SB method is performed at the initial, intermediate, and final levels to capture the textural variations between the parasite and regular artifacts [38]. The developed Boosted-BR-STM is depicted in Figure 3.

The Boosted-BR-STM learns abstract and target levels with various characteristics by carefully arranging three STM blocks with a similar topology. Each block comprises four dilated-convolutional blocks, where regional and edge operations are used by appropriately applying max and average pooling within each convolutional block [39,40], as shown in the equations (1-3). This systematic implementation aids in efficiently exploring border or edge determination, regional homogenous, and textural variation of parasitic and artifact images.

$$x_{k,l} = \sum_{i=1}^m \sum_{j=1}^n x_{k+i-1,l+n-1} f_{i,j} \quad (1)$$

$$x_{k,l}^{\max} = \max_{i=1,\dots,w,j=1,\dots,w} x_{k+i-1,l+j-1} \quad (2)$$

$$x_{k,l}^{\text{avg}} = \frac{1}{w^2} \sum_{i=1}^w \sum_{j=1}^w x_{k+i-1,l+j-1} \quad (3)$$

In the equation, ' \mathbf{x} ' represents the input feature map, size is shown with the symbols ' k ' x ' l ' and ' I ' x ' j ', and ' f ' stands for the filter (1) in equations (2-3). As indicated in the equation, every one of the four convolutional blocks (B, C, D, and E) uses channel SB differently to learn distinct parasitic feature sets (4). While learning blocks D and E from scratch, TL builds additional channels in blocks B and C to provide different feature maps. Each STM convolutional block has 32, 64, 128, and 128, 256, 512 channel dimensions when squeezed and boosted, correspondingly [41]. TL's core role is to gain information from the trained source-domain and solve issues in the target-domain while pursuing a high level of performance. Block A also uses region smoothing techniques to minimize the distortion and outlier acquired while capturing the input images [42]. The boosted channel is handled in block F to lessen connection intensity and obtain ideal attributes.

$$\mathbf{x}_{\text{Boosted}} = b(\mathbf{x}_B || \mathbf{x}_C || \mathbf{x}_D || \mathbf{x}_E) \quad (4)$$

$$\mathbf{x} = \sum_a^A \sum_b^B v_a \mathbf{x}_{\text{Boosted}} \quad (5)$$

$$\sigma(\mathbf{x}) = \frac{e^{x_i}}{\sum_{i=1}^c e^{x_c}} \quad (6)$$

The feature-maps of block D and E are denoted in equation (4) by the variables x_D and x_E , respectively. Likewise, blocks B and C is based on additional channels created using TL and are shown as x_B and x_C , respectively. $b(\cdot)$ represents the boosting operation $b(\cdot)$. Additionally, the developed CNN employs fully

connected layers with dropout layers to collect and preserve target-specific features and minimize overfitting. V serve as an example of the number of neurons in equation (5). Lastly, equation (6), whereas c stands for the no of classes, represents softmax, an activation function.

Significance of using Auxiliary Channels

The representative capability of the proposed hybrid framework is enhanced by adding numerous additional channels in deep the developed Boosted-BR-STM and ensemble learning. The deep CNNs used to create auxiliary channels are TL based; they are initially squeezed to get salient channels and combined with each STM block at abstract, mid, and high levels. Concatenating the prominent and notable information from various deep CNNs using distinct channels enhances the malaria infection depiction. The developed SB-based deep-CNN learns intricate local and global patterns to differentiate between texture variations in parasitic and healthy samples.

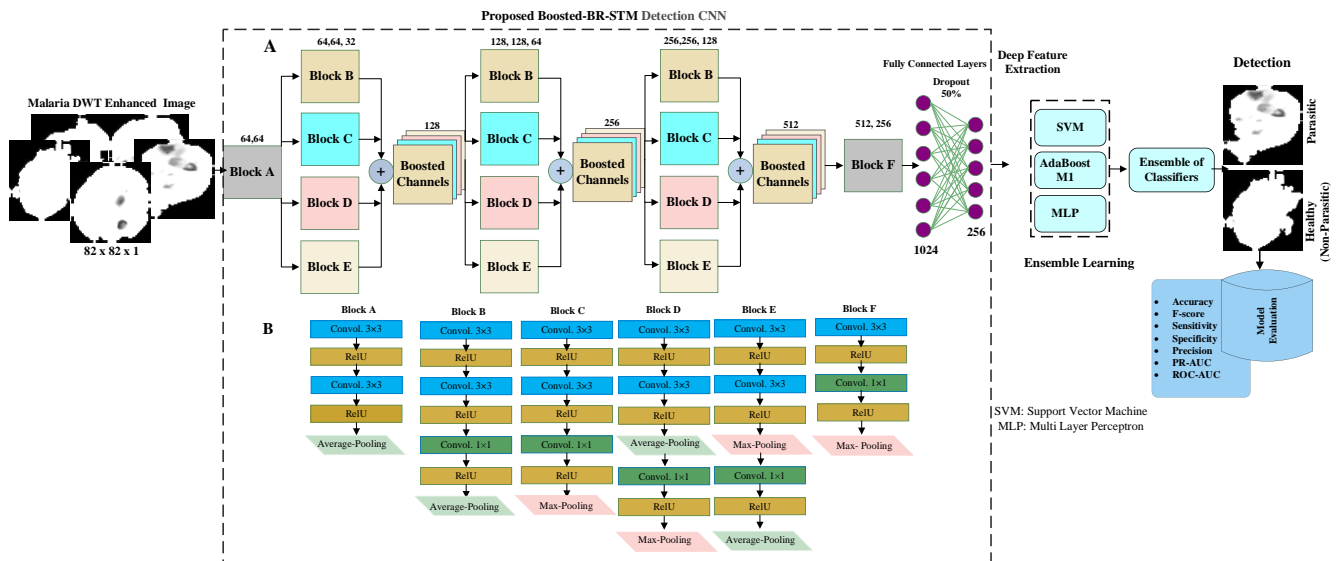


Figure 3 The proposed malaria parasite detection framework comprised the developed Boosted-BR-STM and Ensemble of Classifiers.

3.3.2. Ensemble Learning

We employ deep boosted feature-maps and classifier ensemble strategies in the proposed hybrid learning. The boosted hybrid learning implicates the boosted feature space given to the ensembling classifiers ML classifier. In addition, ensemble classifiers combine decisions from various classifiers that depend on a voting strategy.

We also used a hybrid learning-based strategy by separating the key characteristics, utilizing the developed deep Boosted-BR-STM learning potential, and combining it with ML classifiers' robust discriminating capabilities. We have taken the deep feature spaces from the boosted deep CNN's last layers and delivered them to competing ML classifiers (SVM [40], MLP [43], and AdaBoostM1 [44]). The proposed DBEL framework extracts deep boosted channels from the proposed Booste-BR-STM to achieve diverse channels and provides to ensemble classifier, as shown in equation (6). Moreover, the DBEL benefits both feature maps boosting and ensemble learning. Finally, the generalized detection model provides deep, rich information feature space [45]. The deep feature maps are generated, the 2nd last fully connected (FC) layer of developed Boosted-BR-STM and customized CNNs and fed to the ML classifier. Ultimately, integrating deep boosting and ensemble classifier improves the DBEL framework generalization ability.

Significance of Hybrid Learning

The training of the proposed deep Boosted-BR-STM and customized CNNs may sometimes cause overfitting. Therefore, the proposed hybrid framework learns the effective discrimination features and improves generalization. Additionally, SVM [40], MLP [43], and AdaBoostM1 [44] represent three distinct ML classifiers that minimize the structural risk. Deep CNNs causes empirical risk by reducing training error using the optimal hyper-parameter selection [40]. The proposed framework significantly reduces both training and test error and thus improve the generalization. Moreover, Ensemble learning aims to increase performance and promotes integrating numerous feature spaces into a single rich information feature vector [46].

3.4. Utilization of Customized CNNs

Several current CNNs like VGG, ResNet, GoogleNet, DenseNet, and Inception have been adapted to classify parasite malaria images for comparative analysis [19,20,27,30,32,33]. The existing CNN's abstract and final classification layers are customized using additional layers according to the input and target-class dimension of the dataset. CNN models were primarily backpropagation strategies learned from scratch where initial weights were randomly selected. The convolutional layers' initial weights were borrowed from pre-train models using TL to improve the model convergence. In this regard, we used TL to adopt effective model parameters derived from the modified prior CNNs designed to

precisely capture the target-domain specific parasite characteristics mostly on the malaria dataset employing improved filter weights acquired from ImageNet [47].

4. Experimental Setup

4.1. Dataset

The NIH dataset separated parasitic cells from a thin blood smear slide for research on monitoring and diagnosis [20]. The dataset includes samples of falciparum patients collected from the Mahidol Oxford Tropical Medicine Center and Bangladesh's Chittagong Medical College [48]. The institutes mentioned above are proficient slide readers who differentiate between parasitic images and healthy individuals. Plasmodium is present mainly in positive (parasitic) specimens, while the artifact effect is seen in negative (non-parasitic or healthy) samples with staining and contaminants. The malaria dataset distribution for experimental setup is shown in Table 2 and Figure 4, pictorially depicting the parasite and non-parasitic or healthy RBC samples.

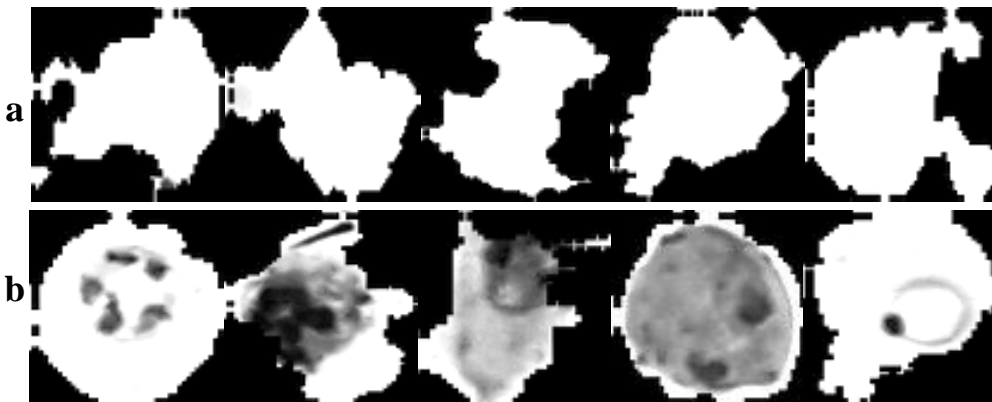


Figure 4 Panel (a, b) DWT enhanced parasitic and normal samples, respectively.

Table 2 Benchmarked NIH Malaria Dataset Detail

Properties	Description
Total	27,558 Images
Non-Parasite (Healthy and Impurities)	13,779 Images
Parasite	13,779 Images
Train and Validation (70%)	(9645, 9645)
Test (30%)	(4134, 4134)
Original dimension	164 x 164 x 3
Enhanced Image Size	82 x 82 x 1

4.2. Model Training

The training and testing parts of the dataset are divided into a 70:30 % ratio. Additionally, cross-validation is executed in the training phase, which is partitioned 80:20 into training and testing sets during model training. The training set includes the data-validation set when optimum parameters are picked via hold-out cross-validation. Table 3 lists the selected optimal parameters in detail. The MATLAB-2021b tool was used to create the modified CNNs. The tests were carried out on an NVIDIA-GeForce GTX-T-Dell PC with 32-GB RAM and CUDA support. CNNs required nearly 12–24 hours during training or 1–2 hours for each epoch.

Table 3 Hold-out based optimal hyper-parameter selection

Hyper-parameter	Values
Learning-rate (α)	10^{-3}
Optimizer	SGD
Epoch	10
Momentum	0.90
Loss	Cross Entropy

4.3. Performance Evaluation

Standard performance criteria are used to evaluate the efficiency of the current CNNs and the developed hybrid learning framework. The detection measures include Accuracy, Precision, Sensitivity, Specificity, and F-score are used as optimization metrics for evaluating the performance of the technique. These measurements, along with a mathematical explanation and abbreviation, are explained in equations 7 to 11.

$$\text{Accuracy} = \frac{\text{Classified Correctly}}{\text{Total Samples}} \times 100 \quad (7)$$

$$\text{Precision} = \frac{\text{Classified Parasitic}}{\text{Classified Parasitic} + \text{Incorrectly Classified Parasitic}} \quad (8)$$

$$\text{Sensitivity} = \frac{\text{Classified Parasitic}}{\text{Total Parasitic Samples}} \quad (9)$$

$$\text{Specificity} = \frac{\text{Classified Healty}}{\text{Total Healty Individuals}} \quad (10)$$

$$\text{F - Score} = 2 \frac{(\text{Sen} \times \text{Pre})}{\text{Sen} + \text{Pre}} \quad (11)$$

5. Results And Discussion

This study uses the original and DWT-improved datasets to establish a novel detection DBEL framework system for malaria to distinguish parasite malaria sufferers from non-parasitic individuals. Moreover, a novel Boosted-BR-STM is developed to test the usefulness of boosting and boundary-region based STM to forecast affected parasite cells in RBC-thin-smears microscopy samples, and its effectiveness is contrasted with modified existing CNNs. Furthermore, the existing CNNs are upgraded and deployed in the TL and trained from scratch. Table 4 shows that the developed malaria detection employing a defined performance metrics is assessed.

5.1. Performance Analysis of Detection Results

5.1.1. Enhanced Dataset Evaluation

Impurities, staining, and noise artifacts in the original malaria dataset generated a striking likeness between images captured with and without parasites. So, pre-processing step is required to remove stains/impurities and impulsive noise from blood smear images. In this case, DWT reduces noise effects, stain impurity, and computing time, attaining streamlined, improved feature channels. Moreover, DWT coefficients preserve important low-resolution and diagonal features that aid in differentiating malaria-infected RBCs from healthy samples. Tables 5 and 6 show how using CNN using enhanced DWT data outperformed the standard dataset in terms of Accuracy (1.86-3.1%), F1-Score (1.8-2.9%), Sensitivity (0.60-2.2%), Precision (2.40-5.50%), Specificity (2.6-6.1%). The minimum, average, and maximum performance for every parameter is displayed in Figure 5. Moreover, DWT is frequently employed as an enhancement approach for data cleaning, significant feature-map generation, and improved classification framework performance.

5.1.2. The Proposed Boosted-BR-STM

The developed Boosted-BR-STM improved the generalizability of the proposed DBEL scheme compared to early methods and yielded better results on a DWT-enhanced test dataset. Table 7 and Figure 5 demonstrated a significant enhancement in the developed Boosted-BR-STM to forecast

plasmodium falciparum-infected patients that exploits homogenous and boundary-driven parasite patterns in the STM block, Boosted, and TL to improve the recall and F1-score.

Region homogenous and boundary characteristics aid in learning the distorted parasitic samples. Moreover, TL-based generated feature-maps and SB can capture subtle contrast and texture variation across artifact and parasite samples. Moreover, data augmentation strategies employed in the training portion yielded performance improvement and model generalization. Furthermore, Accuracy and precision are attained by decreasing false positives, which reduces the medical staff's workload significantly. Tables demonstrates the Boosted-BR-STM fared better than reported approaches to the identical NIH dataset. The Boosted-BR-STM performs better than other methods; Accuracy values range from (1.16-7.44 %), F-score (1.2-7.5 %), and Sensitivity (2.5-4.8 %). The developed Boosted-BR-STM lower False Negative (FN=71) and improved sensitivity relative to the finest, most reputable TL-based DenseNet CNN (FN=131) on unseen DWT enhanced dataset, as demonstrated in Table 5 and Table 6.

Table 4 Performance of Boosted-BR-STM and existing CNNs on unseen dataset

Models	Trained from scratch (Original-Data)				
	Accuracy %	F-score	Sensitivity	Precision	Specificity
ShuffleNet	92.85	0.931	0.965	0.899	0.892
ResNet-50	94.96	0.951	0.980	0.924	0.919
SqueezeNet	95.16	0.953	0.976	0.931	0.928
Inceptionv3	95.40	0.955	0.980	0.931	0.928
ResNet-18	95.66	0.958	0.986	0.931	0.927
Xception	95.22	0.953	0.969	0.938	0.936
DenseNet-201	95.73	0.958	0.978	0.939	0.936
VGG-19	95.74	0.958	0.966	0.950	0.949
VGG-16	95.79	0.958	0.965	0.951	0.95
GoogleNet	95.23	0.953	0.960	0.946	0.945
Proposed Boosted-BR-STM	96.67	0.967	0.986	0.949	0.901

Table 5 Performance comparison of Boosted-BR-STM and existing CNNs on unseen dataset.

Models	Trained from scratch on Enhanced Data (DWT)				
	Accuracy %	F-score	Sensitivity	Precision	Specificity
ShuffleNet	94.71	0.949	0.976	0.923	0.918
SqueezeNet	95.34	0.954	0.969	0.940	0.938
Inceptionv3	95.43	0.955	0.966	0.944	0.942
ResNet-50	95.55	0.956	0.969	0.944	0.942
Xception	95.67	0.957	0.980	0.936	0.933
ResNet-18	95.71	0.958	0.969	0.947	0.945
VGG-16	95.80	0.958	0.971	0.946	0.945
DenseNet-201	95.84	0.959	0.973	0.945	0.944
GoogleNet	95.85	0.959	0.982	0.938	0.935
VGG-19	95.95	0.960	0.966	0.954	0.953
Proposed Boosted-BR-STM	97.51	0.975	0.982	0.968	0.968

Table 6 TL-based existing CNNs performance analysis

Models	TL-based CNNs				
	Accuracy %	F-score	Sensitivity	Precision	Specificity
SqueezeNet	95.08	0.952	0.978	0.927	0.923
ShuffleNet	95.71	0.957	0.971	0.944	0.943
VGG-19	95.79	0.958	0.969	0.948	0.947
Inceptionv3	95.91	0.959	0.971	0.948	0.947
GoogleNet	96.03	0.962	0.983	0.941	0.938
Xception	96.07	0.961	0.971	0.951	0.95
ResNet-50	96.17	0.962	0.974	0.951	0.949
VGG-16	96.2	0.962	0.975	0.95	0.949
ResNet-18	96.21	0.963	0.985	0.942	0.94
DenseNet-201	96.31	0.963	0.968	0.958	0.958

5.1.3. The Proposed Hybrid Learning

The malaria parasite samples are diagnosed using a new deep-boosted feature-map and ensemble learning (DBEL). In this regard, three competing ML classifiers are ensembled with feature vectors of the proposed Boosted-BR-STM that contribute as feature extractors. Moreover, the malaria parasitic images are detected by extracting the deep features from existing CNNs and providing them to ML classifiers in the DHML scheme. The significance of exploiting deep features is identified and compared with Softmax-based evaluation. The DHML using TL-based fine-tuned existing CNNs scheme outperforms Softmax-based evaluation in terms of Accuracy (0.47-1.7%), F1-Score (0.50-1.6%), Precision (0.50-3.6%), Specificity (0.5-4%), as illustrated in Table 4.

5.1.4. The proposed DBEL Framework

The hybrid learning approach evaluates the performance of deep-boosted feature maps and ensemble learning. The proposed DBEL outperformed the customized CNNs by providing a deep-boosted feature map to the majority voting-based ensembled classifiers. Combining boosted deep feature maps and utilizing three classifiers creates a hybrid of diverse feature spaces and ensemble learning. Boosting learning aims to increase performance and promotes integrating numerous feature spaces into a single rich information feature vector [38]. Moreover, the ensemble classifiers' improves the proposed framework's differentiation capacity by merging deep feature maps to construct the boosted and diverse feature space. The metrics used to evaluate performance are accuracy, recall, F-score, etc. Finally, the proposed DBEL framework outperformed the existing techniques for classifying malaria parasite samples in terms of Accuracy (1.72-5.65%), F1-Score (1.70-5.4%), Precision (1.60-8 %), Specificity

(1.5-8.6%), as shown in Table 8. Finally, the proposed DBEL framework's further reduced the FN (34), as contrasted to the best and most reputable DenseNet CNN. However, a few samples were missed due to a similarity between malaria-infected and healthy people owing to impurity, stain, or noise anomalies in non-parasitic instances, as seen in Figure 7.

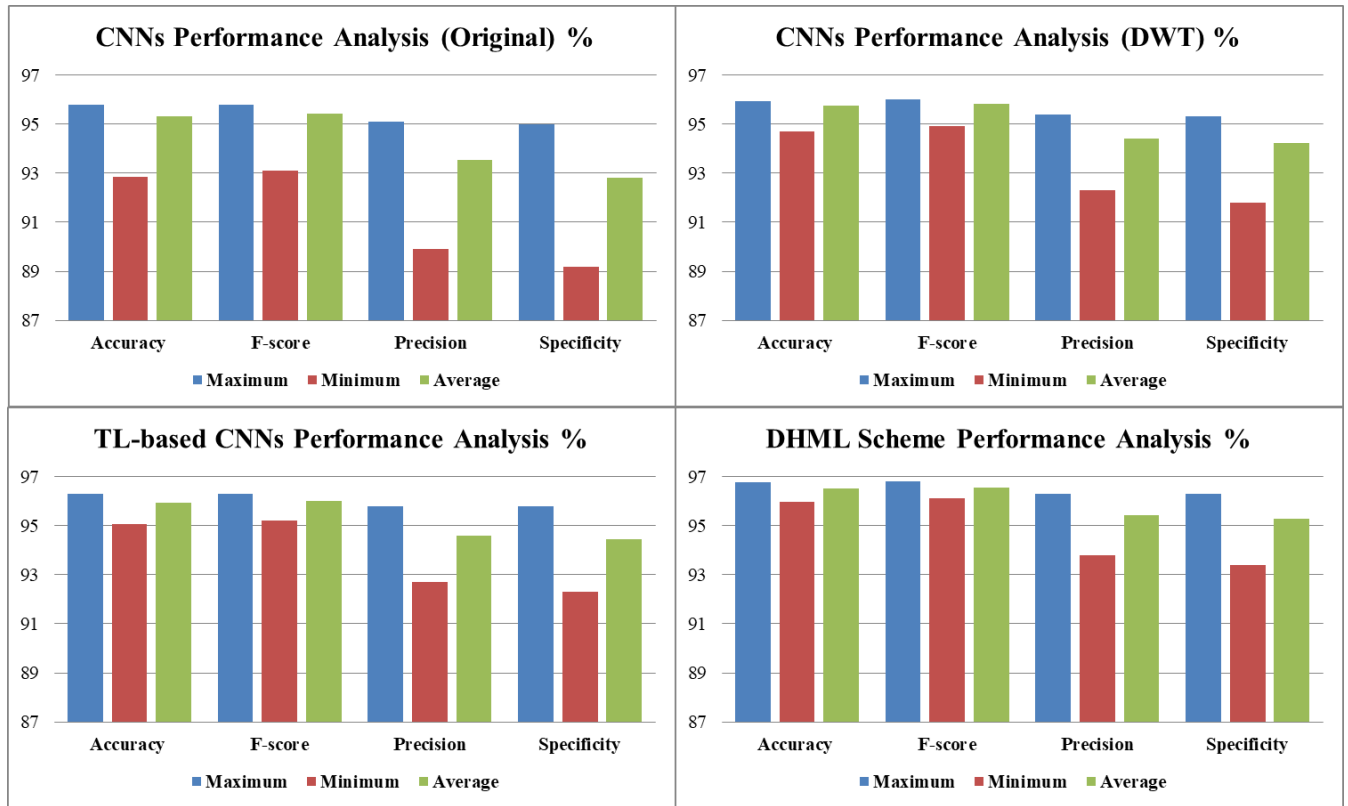


Figure 5 The DHML framework outperforms current CNNs (trained from scratch and TL). Moreover, an enhanced DWT samples considerably improved performance.

Table 7 Performance analysis of TL-based existing CNNs Deep Feature and ML.

Models	TL-based DHML Scheme				
	Accuracy %	F-score	Sensitivity	Precision	Specificity
SqueezeNet	95.96	0.961	0.985	0.938	0.934
ShuffleNet	96.26	0.963	0.969	0.957	0.956
VGG-19	96.34	0.964	0.974	0.954	0.953
Inceptionv3	96.48	0.965	0.975	0.956	0.955
GoogleNet	96.57	0.966	0.975	0.957	0.956
Xception	96.65	0.967	0.980	0.955	0.953
ResNet-50	96.65	0.967	0.983	0.952	0.950
VGG-16	96.69	0.967	0.971	0.963	0.963
ResNet-18	96.70	0.968	0.982	0.954	0.952
DenseNet-201	96.78	0.968	0.978	0.958	0.957

Table 8 Performance analysis of the proposed frameworks

Framework	The Proposed DBEL Framework Work				
	Accuracy %	F-score	Sensitivity	Precision	Specificity
Deep Boosted Machine Learning					
SVM	97.73	0.977	0.985	0.970	0.969
AdaboostM1	97.92	0.979	0.988	0.971	0.971
MLP	98.08	0.981	0.988	0.974	0.973
Deep Boosted Ensemble Learning					
SVM + AdaboostM1	98.21	0.982	0.991	0.974	0.973
AdaboostM1+MLP	98.26	0.982	0.99	0.975	0.975
MLP+ SVM	98.34	0.983	0.991	0.976	0.976
Proposed DBEL (SVM + AdaboostM1+ MLP)	98.50	0.985	0.992	0.979	0.978

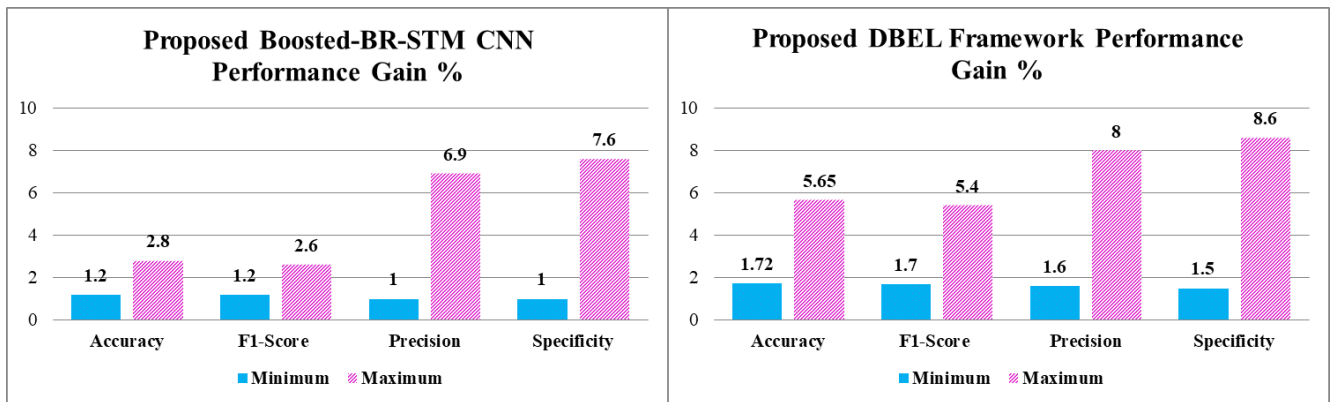


Figure 6 The proposed Boosted-BR-STM CNN and DBEL framework performance gain over the existing detection

5.1.5. Customized CNNs

TL is an essential DL technique to perform satisfactorily instead of training CNN from scratch. TL adopted custom CNNs utilizing DWT-enriched data outperformed learning from scratch, as shown in Table 7. The TL-based fine-tuned existing CNNs perform better than those learned from scratch and existing techniques: Accuracy (0.36-1.6%), F1-Score (0.30-1.4%), Sensitivity (0.30-1.9%), Precision (0.40-3.5%), and Specificity (0.5-4%). Tables 5 and 6 show the comparative study with customized deep-CNN models, along with Figure 5. TL enhanced the CNN learning convergence through pattern initialization and thus, lowering the miss-classification rate while maintaining precision. This demonstrates TL's ability to analyze medical image fields, especially malaria detection.

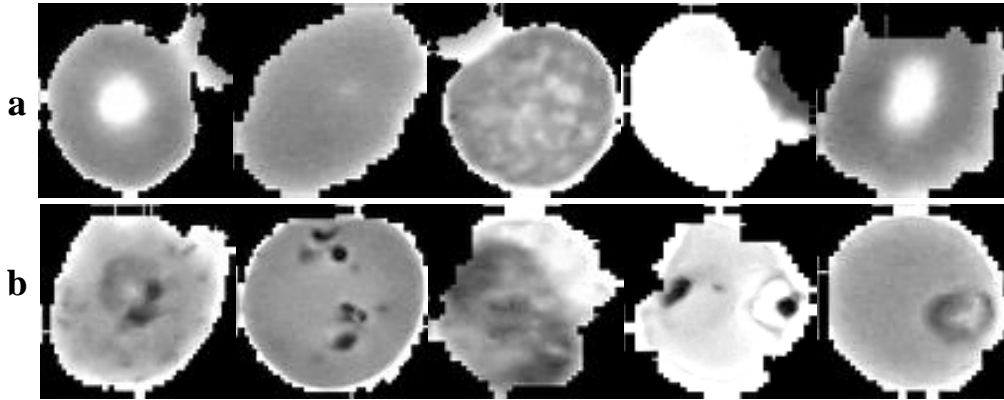


Figure 7 The enhanced stain artifacts and parasitic samples are shown in panels (a) and (b). The parasite images have a high degree of resemblance to artifacts, resulting in a high rate of miss detection

Table 9 The proposed framework performance comparison with the recent techniques used the NIH Malaria datasets

Techniques	Accuracy %	F-score	Sensitivity	Precision	Specificity
Dense-Net [19]	90.54	0.9050	0.9400	0.9080	0.8770
Inception [19]	93.06	0.9306	0.9300	0.9306	0.9310
Xception [19]	94.94	0.9490	0.9260	0.9510	0.9750
Customized ResNet-50 [33]	95.40	---	---	---	---
Sequential-CNN [20]	95.90	0.9590	0.9470	---	0.9720
VGG-16 [32]	95.96	0.9560	---	0.9680	---
Proposed DBEL Framework	98.50	0.985	0.992	0.979	0.978

5.2. Feature Space Visualization

The distinct class samples enhanced the ability of model learning and robustness. Therefore, the principal components analysis (PCA) aims to depict the significant discriminative features. The top-2 (PC1 vs. PC2) distinct components of the test samples are displayed in Figure 8, with distinctive coloring for every feature point for distinguishing parasite-containing samples from non-parasitic ones [49,50]. The feature space is examined to better comprehend the proposed Boosted-STM decision-making BR's behavior in contrast to the existing DenseNet-201 model.

The developed Boosted-BR-STM's generated feature space depicts the discrimination among parasite and healthy samples, as illustrated in Figure 8 and Figure 9. The Boosted-BR-STM has the highest evaluating effectiveness, according to the 2D PC plots. While the current CNN DenseNet-201 has discovered that feature spaces are cluttered and inaccurately unable to distinguish between two classes using the original data. Additionally, compared to DenseNet-201 trained from scratch using improved DWT data, TL-based DenseNet-201 better indicates the instance class.

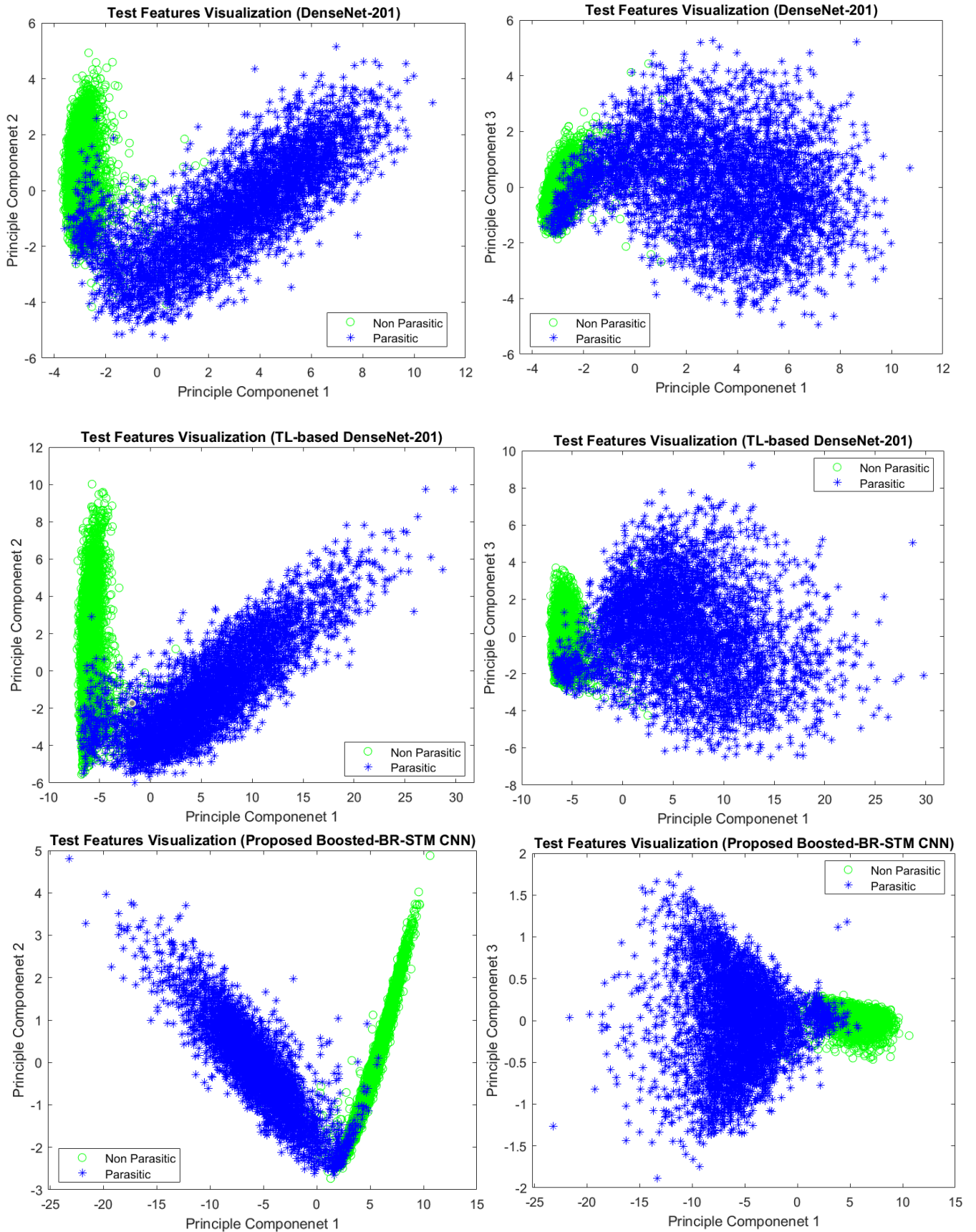


Figure 8 Test distinct feature visualization PC1, PC2, and PC3 for the developed Boosted-BR-STM contrasts DenseNet-201.

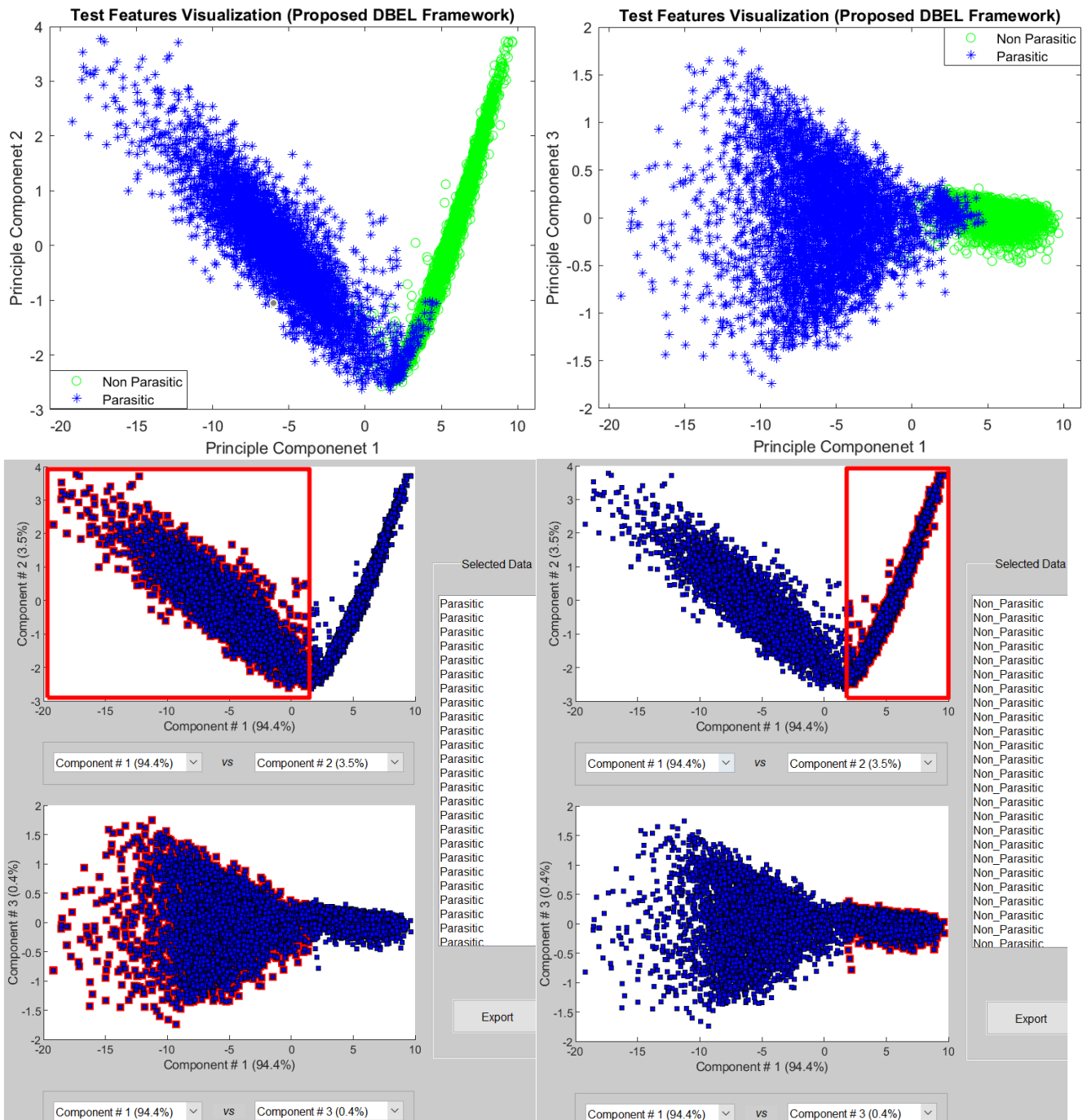


Figure 9 The visualization for the generated of PC1, PC2, and PC3 distinct features for the proposed DBEL on DWT-enriched datasets.

5.3. Graphical Analysis

The sensitivity and precision metrics for assessing the models are critical for malaria parasite detection. Therefore, Precision-recall (PR) and receiver-operating curve (ROC) are drawn for the developed DBEL framework, Boosted-BR-STM and customized CNNs on test data. These graphs depict the

capability of the classifier to differentiate across various potential ranges. The detection cut-off of the best positive class classifier can be considerably accessed via ROC and PR curves; results are shown in Figure 10 [51]. The Boosted-BR-STM reduced false-negative or miss-classified parasitic compared to existing CNNs on an enhanced dataset with a PR AUC=99.5 % [52]. Moreover, the developed DBEL framework maintains minimal false-positives by detecting malarial infections with strong sensitivity due to its high ROC-AUC value.

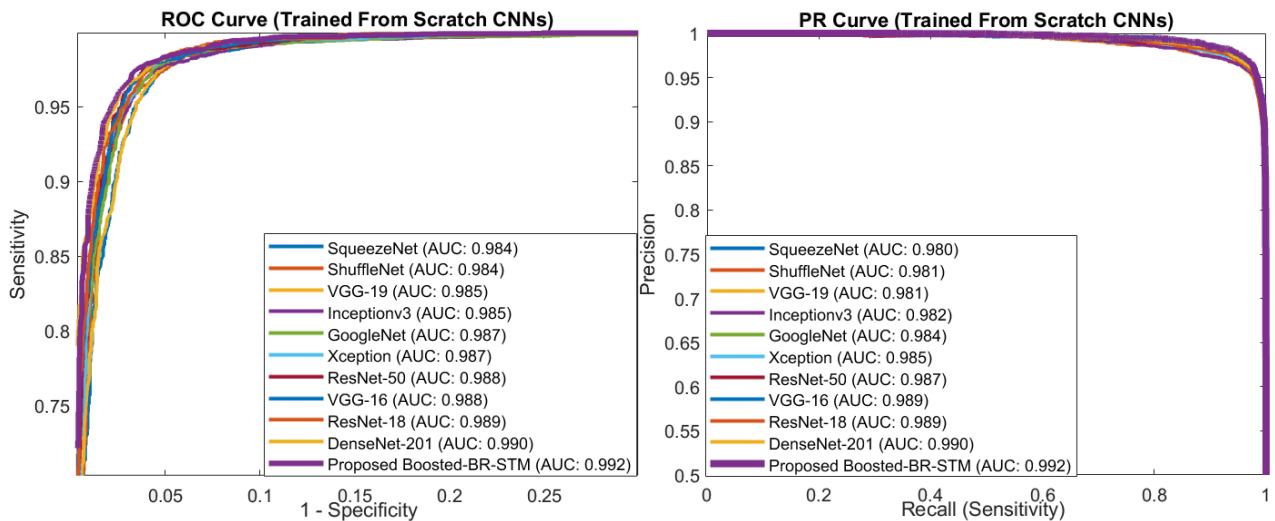


Figure 10 The developed Boosted-BR-STM with TL-based fine-tuned CNN's ROC and PR curves on original and DWT enriched data.

6. Conclusion

The proposed hybrid DBEL framework stack deep boosted features of the developed Boosted-BR-STM CNN and ensemble learning to detect RBC thin smears microscope images of malaria patients. The proposed DBEL framework benefits from DWT enhancements, data augmentation, incorporating TL, inherent discriminative deep features from the developed Boosted-BR-STM, and ensemble learning to improve classification performance. Moreover, the developed Boosted-BR-STM employs TL for the diverse rich information feature-maps generation and squeezing-boosting ideas in STM block, improving the capability to learn homogeneity, textural variation, and parasitic structural patterns. The proposed framework achieved the accuracy of 98.50 %, an AUC of 0.996, an F-score of 0.985, and a sensitivity of 0.992. Furthermore, the proposed Boosted-BR-STM and framework excelled in existing techniques, experimentally in correctly detecting malaria-infected patients. In the future, the proposed DBEL is intended to help healthcare practitioners automatically detect parasitic malaria patients for

clinical examination. Furthermore, the developed framework can be employed in diagnosing brain tumors, lung cancer, and breast cancer using medical images.

Acknowledgment

We thank Department of Computer Systems Engineering, University of Engineering, and Applied Sciences (UEAS), for providing necessary computational resources and a healthy research environment.

References

1. Keleta Y, Ramelow J, Cui L, Li J. Molecular interactions between parasite and mosquito during midgut invasion as targets to block malaria transmission. *npj Vaccines*. 2021.
2. Gupta S, Gazendam N, Farina JM, Saldarriaga C, Mendoza I, López-Santi R, et al. Malaria and the Heart: JACC State-of-the-Art Review. *J. Am. Coll. Cardiol*. 2021. p. 1110–21.
3. Yimam Y, Nateghpour M, Mohebbali M, Afshar MJA. A systematic review and meta-analysis of asymptomatic malaria infection in pregnant women in Sub-Saharan Africa: A challenge for malaria elimination efforts. *PLoS One*. 2021.
4. Tegegne Y, Worede A, Derso A, Ambachew S. The Prevalence of Malaria among Children in Ethiopia: A Systematic Review and Meta-Analysis. *J. Parasitol. Res*. 2021.
5. World Health Organization (WHO). WHO Malaria Policy Advisory Group (MPAG) meeting. 2021. p. 13–4.
6. Abbas N, Saba T, Rehman A, Mehmood Z, Javaid N, Tahir M, et al. Plasmodium species aware based quantification of malaria parasitemia in light microscopy thin blood smear. *Microsc. Res. Tech*. 2019. p. 1198–214.
7. Yoon J, Jang WS, Nam J, Mihn DC, Lim CS. An automated microscopic Malaria parasite detection system using digital image analysis. *Diagnostics*. 2021.
8. Barber BE, William T, Grigg MJ, Yeo TW, Anstey NM. Limitations of microscopy to differentiate Plasmodium species in a region co-endemic for Plasmodium falciparum, Plasmodium vivax and Plasmodium knowlesi. *Malar J* [Internet]. 2013;12:8. Available from: <https://malariajournal.biomedcentral.com/articles/10.1186/1475-2875-12-8>
9. Mukry SN, Saud M, Sufaida G, Shaikh K, Naz A, Shamsi TS. Laboratory diagnosis of malaria: Comparison of manual and automated diagnostic tests. *Can. J. Infect. Dis. Med. Microbiol*. 2017.
10. Maity M, Gantait K, Mukherjee A, Chatterjee J. Visible spectrum-based classification of malaria blood samples on handheld spectrometer. *I2MTC 2019 - 2019 IEEE Int. Instrum. Meas. Technol. Conf. Proc*. 2019.
11. Microwave A, Engineering E. *Software / Diagnostic Manual*. p. 1–8.
12. Somasekar J, Sharma A, Madhusudhana Reddy N, Padmanabha Reddy YCA. Image analysis for automatic enumeration of rbc infected with plasmodium parasites-implications for malaria diagnosis. *Adv. Math. Sci. J*. 2020. p. 1229–37.
13. Krishnadas P, Sampathila N. Automated Detection of Malaria implemented by Deep Learning in Pytorch. 2021 IEEE Int Conf Electron Comput Commun Technol [Internet]. IEEE; 2021. p. 01–5. Available from: <https://ieeexplore.ieee.org/document/9622608/>
14. Kalkan SC, Sahingoz OK. Deep learning based classification of malaria from slide images. 2019 Sci. Meet. Electr. Biomed. Eng. Comput. Sci. EBBT 2019. 2019.
15. Khan A, Khan SH, Saif M, Batool A, Sohail A, Khan MW. A Survey of Deep Learning Techniques for the Analysis of COVID-19 and their usability for Detecting Omicron. 2022; Available from: <http://arxiv.org/abs/2202.06372>
16. Du X, Wang X, Xu F, Zhang J, Huo Y, Ni G, et al. Morphological components detection for super-depth-of-field bio-micrograph based on deep learning. *Microscopy*. 2022. p. 50–9.
17. Zafar MM, Rauf Z, Sohail A, Khan AR, Obaidullah M, Khan SH, et al. Detection of tumour infiltrating lymphocytes in CD3 and CD8 stained histopathological images using a two-phase deep CNN. *Photodiagnosis Photodyn Ther* [Internet]. 2022;37:102676. Available from: <https://linkinghub.elsevier.com/retrieve/pii/S1572100021004932>
18. Abubakar A, Ajuji M, Yahya IU. DeepFMD: Computational Analysis for Malaria Detection in Blood-Smear Images Using Deep-Learning Features. *Appl Syst Innov* [Internet]. 2021;4:82. Available from: <https://www.mdpi.com/2571-5577/4/4/82>
19. Maqsood A, Farid MS, Khan MH, Grzegorzec M. Deep malaria parasite detection in thin blood

smear microscopic images. *Appl. Sci.* 2021. p. 1–19.

20. Rajaraman S, Antani SK, Poostchi M, Silamut K, Hossain MA, Maude RJ, et al. Pre-trained convolutional neural networks as feature extractors toward improved malaria parasite detection in thin blood smear images. *PeerJ.* 2018.

21. Das DK, Ghosh M, Pal M, Maiti AK, Chakraborty C. Machine learning approach for automated screening of malaria parasite using light microscopic images. *Micron.* 2013. p. 97–106.

22. Sarkar RP, Maiti A. Investigation of dataset from diabetic retinopathy through discernibility-based k-NN algorithm. *Adv. Intell. Syst. Comput.* 2019. p. 93–100.

23. T. Colwell WBMCS. Automated Detection of *P. falciparum* Using Machine Learning Algorithms with Quantitative Phase Images of Unstained Cells. Sullivan DJ, editor. *PLoS One* [Internet]. 2016;11:e0163045. Available from: <https://dx.plos.org/10.1371/journal.pone.0163045>

24. T. G, J.H. K, H. B, S.J. L. Machine learning-based in-line holographic sensing of unstained malaria-infected red blood cells [Internet]. *J. Biophotonics.* 2018. p. e201800101. Available from: <http://www.embase.com/search/results?subaction=viewrecord&from=export&id=L629306704%0Ahttp://dx.doi.org/10.1002/jbio.201800101>

25. Mehanian C, Jaiswal M, Delahunt C, Thompson C, Horning M, Hu L, et al. Computer-Automated Malaria Diagnosis and Quantitation Using Convolutional Neural Networks. *Proc. - 2017 IEEE Int. Conf. Comput. Vis. Work. ICCVW 2017.* 2017. p. 116–25.

26. Bibin D, Nair MS, Punitha P. Malaria Parasite Detection from Peripheral Blood Smear Images Using Deep Belief Networks. *IEEE Access.* 2017. p. 9099–108.

27. Var E, Boray Tek F. Malaria Parasite Detection with Deep Transfer Learning. *UBMK 2018 - 3rd Int. Conf. Comput. Sci. Eng.* 2018. p. 298–302.

28. Dong Y, Jiang Z, Shen H, David Pan W, Williams LA, Reddy VVB, et al. Evaluations of deep convolutional neural networks for automatic identification of malaria infected cells. *2017 IEEE EMBS Int. Conf. Biomed. Heal. Informatics, BHI 2017.* 2017. p. 101–4.

29. Lenet-5, convolutional neural networks. 2015.

30. Szegedy C, Wei Liu, Yangqing Jia, Sermanet P, Reed S, Anguelov D, et al. Going deeper with convolutions. *2015 IEEE Conf Comput Vis Pattern Recognit. IEEE;* 2015. p. 1–9.

31. Hung, Jane, Allen Goodman, Stefanie Lopes, Carpenter A. Applying Faster R-CNN for Object Detection on Malaria Images. *J R Stat Soc Ser A Stat Soc.* 2013. p. 417–33.

32. Huq A, Pervin MT. Robust Deep Neural Network Model for Identification of Malaria Parasites in Cell Images. *2020 IEEE Reg. 10 Symp. TENSYP 2020.* 2020. p. 1456–9.

33. Reddy ASB, Juliet DS. Transfer Learning with ResNet-50 for Malaria Cell-Image Classification. *2019 Int Conf Commun Signal Process* [Internet]. Boston, MA: IEEE; 2019. p. 0945–9. Available from: <https://ieeexplore.ieee.org/abstract/document/8697909/>

34. Houwen B. Blood film preparation and staining procedures. *Clin. Lab. Med.* 2002. p. 1–14.

35. Sakthidasan alias Sankaran K, Nagarajan V. Noise Removal Through the Exploration of Subjective and Apparent Denoised Patches Using Discrete Wavelet Transform. *IETE J. Res.* 2021. p. 843–52.

36. Pandit P, Anand A. Diagnosis of Malaria Using Wavelet Coefficients and Dynamic Time Warping. *Int. J. Appl. Comput. Math.* 2019.

37. Shorten C, Khoshgoftaar TM. A survey on Image Data Augmentation for Deep Learning. *J. Big Data.* 2019.

38. Khan SH, Shah NS, Nuzhat R, Majid A, Alquhayz H, Khan A. Malaria parasite classification framework using a novel channel squeezed and boosted CNN. *Microscopy* [Internet]. 2022; Available from: <https://academic.oup.com/jmicro/advance-article/doi/10.1093/jmicro/dfac027/6594948>

39. Khan SH, Sohail A, Zafar MM, Khan A. Coronavirus disease analysis using chest X-ray images and a novel deep convolutional neural network. *Photodiagnosis Photodyn Ther* [Internet]. 2021;35:102473. Available from: <https://linkinghub.elsevier.com/retrieve/pii/S1572100021002970>

40. Khan SH, Sohail A, Khan A, Hassan M, Lee YS, Alam J, et al. COVID-19 detection in chest X-ray images using deep boosted hybrid learning. *Comput. Biol. Med.* 2021.
41. Aziz A, Sohail A, Fahad L, Burhan M, Wahab N, Khan A. Channel Boosted Convolutional Neural Network for Classification of Mitotic Nuclei using Histopathological Images. *Proc 2020 17th Int Bhurban Conf Appl Sci Technol IBCAST 2020.* 2020.
42. Khan SH. COVID-19 Detection and Analysis From Lung CT Images using Novel Channel Boosted CNNs. 2022; Available from: <http://arxiv.org/abs/2209.10963>
43. Gardner M., Dorling S. Artificial neural networks (the multilayer perceptron)—a review of applications in the atmospheric sciences. *Atmos Environ [Internet].* 1998;32:2627–36. Available from: <https://linkinghub.elsevier.com/retrieve/pii/S1352231097004470>
44. CAO Y, MIAO Q-G, LIU J-C, GAO L. Advance and Prospects of AdaBoost Algorithm. *Acta Autom Sin [Internet].* 2013;39:745–58. Available from: <https://linkinghub.elsevier.com/retrieve/pii/S187410291360052X>
45. Zahoor MM, Qureshi SA, Bibi S, Khan SH, Khan A, Ghafoor U, et al. A New Deep Hybrid Boosted and Ensemble Learning-Based Brain Tumor Analysis Using MRI. *Sensors [Internet].* 2022;22:2726. Available from: <https://www.mdpi.com/1424-8220/22/7/2726>
46. Ganaie MA, Hu M, Tanveer* M, Suganthan* PN. Ensemble deep learning: A review [Internet]. 2021. Available from: <http://arxiv.org/abs/2104.02395>
47. Khan SH, Khan A, Lee YS, Hassan M, Jeong WK. Segmentation of shoulder muscle MRI using a new Region and Edge based Deep Auto-Encoder. *Multimed Tools Appl [Internet].* 2022; Available from: <https://link.springer.com/10.1007/s11042-022-14061-x>
48. Maude RJ, Hasan MU, Hossain MA, Sayeed AA, Kanti Paul S, Rahman W, et al. Temporal trends in severe malaria in Chittagong, Bangladesh. *Malar. J.* 2012.
49. Lobo SA, Siswadi, Bakhtiar T. Visualization of classified data with kernel principal component analysis. *Glob. J. Pure Appl. Math.* 2015. p. 2347–56.
50. Barshan E, Ghodsi A, Azimifar Z, Zolghadri Jahromi M. Supervised principal component analysis: Visualization, classification and regression on subspaces and submanifolds. *Pattern Recognit.* 2011. p. 1357–71.
51. Hajian-Tilaki K. Receiver operating characteristic (ROC) curve analysis for medical diagnostic test evaluation. *Casp. J. Intern. Med.* 2013. p. 627–35.
52. Boyd K, Eng KH, Page CD. Area under the precision-recall curve: Point estimates and confidence intervals. *Lect. Notes Comput. Sci. (including Subser. Lect. Notes Artif. Intell. Lect. Notes Bioinformatics).* 2013. p. 451–66.